Materials Today Communications 37 (2023) 107644

Contents lists available at ScienceDirect

Materials Today Communications

journal homepage: www.elsevier.com/locate/mtcomm

Cracking mechanisms and effect of extensive preheating in CM247LC and IN713LC Ni-base superalloy processed by Laser Powder Bed Fusion

Marawan Abdelwahed [a,b], José Ramón Blasco Puchades [c], Luis Portolés Griñán [c], Mario Martínez Ceniceros [c], Ludovica Rovatti [a], Rasheed Michael Ishola [a], Maurizio Vedani [a,*]

[a] Politecnico di Milano, Department of Mechanical Engineering, Milan, Italy
[b] Ain Shams University, Faculty of Engineering, Design and Production Engineering Department, Cairo, Egypt
[c] AIDIMME, Metal Processing, Furniture, Wood and Packaging Technology Institute, Valencia, Spain

ARTICLE INFO

Keywords:
Ni-superalloy
Laser Powder Bed Fusion
Hot cracking
Preheating

ABSTRACT

Laser powder bed fusion processing of non-weldable γ'-strengthened Ni-based superalloys is challenging due to various cracking mechanisms that occur during the solidification and cooling stages of the materials. The current study offers an insight into the failure mechanisms of the CM247LC and IN713LC alloys, identifying the pre-heating temperatures which can mitigate cracking phenomena during processing. The adopted methodology involved the alloy processing by a standard Laser powder bed fusion system followed by microstructural characterization. It was confirmed that the development of cracks with a length in the range of 100–500 μm became evident in both alloys. High-temperature preheating strategies were then investigated using a simplified approach based on single laser track remelting. At pre-heating levels up to about 900 °C, corresponding to measured cooling rates of the order of 10^4 °C/s, hot cracks were still observed in the alloys due to γ' precipitation and segregation of carbide former elements at the cell boundaries according to both microstructure observations and thermodynamic predictions. Preheating conditions at higher temperatures targeting levels above the γ'-solvus temperature, exceeding 1200 °C could promote slower cooling rates, leading to full suppression of cracks in the investigated γ'-strengthened alloys.

1. Introduction

Laser powder bed fusion, also known with the acronym suggested by ISO/ASTM standards of PBF-LB/M, allows fabricating complex and near-net shape products with minimal material waste and short lead times [1]. These capabilities can lead to significant advantages in the design of high-temperature parts such as blades for gas turbine engines implementing advanced cooling channel configurations that could increase the service temperature, hence the system efficiency. The reference materials for this field are Ni-based superalloys due to their excellent creep and oxidation resistance, low fatigue crack growth rate, and high yield strength at the service temperature. The alloys providing the highest performance are typically strengthened by ordered, coherent γ'-Ni_3(Al,Ti) or γ''-Ni_3Nb precipitates, as for IN738, CMSX-4, CM247LC, and IN713LC alloys [2,3]. However, the attractive service properties of these alloys are achieved at the cost of their processability. It has been established that, similarly to what is found in welding metallurgy, high contents of Al and Ti in the alloys increase the cracking susceptibility and therefore impair the ability to produce defect-free parts by PBF-LB [3–5]. Different mechanisms have been recognized as the possible root causes of the cracking phenomena. Solidification cracking and liquation cracking involve the presence of a liquid film at dendrite boundaries in the last stages of solidification or when the material is re-heated and exposed to temperatures high enough to melt constituents at grain boundaries in presence of residual stresses. In addition, strain-age cracking and ductility-dip cracking could also take place during the solid-stage cooling, after solidification [4–6].

Detailed studies have been published in the open literature about the mechanisms of crack formation during laser beam welding (LBW), electron beam powder bed fusion (PBF-EB), and PBF-LB for some of the most popular γ'-strengthened Ni-based superalloys. Chauvet and co-workers [3] reported that EB-PBF processing of a Ni-Co-Cr-Mo-Al-Ti-B alloy resulted in intergranular cracking along columnar grains featuring high-angle misorientation and Cr-and Mo-rich boride particles at their boundaries. Analyses of the crack surfaces showed that they developed in presence of liquid, suggesting the possible mechanisms of

* Corresponding author.
E-mail address: maurizio.vedani@polimi.it (M. Vedani).

https://doi.org/10.1016/j.mtcomm.2023.107644
Received 31 July 2023; Received in revised form 25 October 2023; Accepted 18 November 2023
Available online 20 November 2023

either solidification cracking or liquation cracking. Wang et al. [7] investigated the PBF-LB processability of the IN738 alloy. The authors attributed cracking to the segregation of Ti at grain boundaries of the as-built structure, which was assumed to promote the formation of the low-melting γ-γ' eutectic. The conclusion was in good agreement with findings derived from the same alloy but processed by laser deposition on directionally solidified substrates published by Chamanfar et al. [8]. Qiu et al. [9] gave evidence of an alternative cracking mechanism for the IN738 alloy associated to the formation of oxygen-rich high-melting phases at grain boundaries.

Raza and Lo [10] as well as Chamanfar et al. [11] investigated the IN713LC alloy, confirming that also for this alloy, the PBF-LB processing and electron beam welding is very challenging due to its cracking susceptibility. Enrichment in Al, Cr, Mo, and Ti close to crack surfaces was detected, supporting the hypothesis of solidification cracking promoted by the formation of low-melting point constituents such as the γ/γ' eutectic. For sake of completeness, it is also worth mentioning that in [10] it was speculated about the additional occurrence of ductility-dip cracking at the solid state due to the re-heating effects of the already deposited material layers.

The CM247LC is a further popular γ'-strengthened Ni-based alloy classified as a non-weldable and non-printable grade. The microstructure and cracking mechanisms developed during PBF-LB and PBF-EB processing have been widely investigated [6,12–17]. Variants of CM247LC such as the DZ125 and the Mar-M247 alloys have also been considered in the literature [18–20]. There is almost full agreement on assigning the main cracking mechanism to a combination of solidification and liquation cracking, often (but not solely) triggered by MC-type carbides [20] or segregation of Hf [6,21], Ta and Nb [19], preferentially at high-angle grain boundaries (HAGBs) of the columnar grains.

It can be stated that the cracking susceptibility of γ'-strengthened Ni-based alloys could be mitigated by a combination of different strategies such as modification of alloy chemistry to reduce the solidification interval and promote liquid backfilling during the last stages of solidification [6,22–25], optimization of process parameters including the adoption of preheating procedures [3,4,6,10,13,18–20], post-processing (e.g. by hot isostatic pressing or Laser shot peening) [4,18,26]. It appears that, despite the remarkable improvements claimed by several authors, none of the listed routes was able to fully remove the cracks upon alloy processing by PBF-LB or PBF-EB.

Particular attention in the present investigation will be given to the effects of high-temperature preheating on solidification cracking mechanisms of the two γ'-strengthened Ni-based alloys CM247LC and IN713LC. Powder bed preheating is considered as a standard procedure for PBF-EB and it has been evaluated in [3,18,19], targeting temperatures in the range of 1025–1050 °C. High-temperature selective laser melting was also investigated by Hagedorn and co-workers with a preheating level of 1200 °C [20]. However, it appears that a detailed investigation on modification and suppression of the cracking mechanisms as a function of the pre-heating level, up to temperatures exceeding 1300 °C is still lacking in the open literature.

2. Materials and methods

Gas-atomized CM247LC and IN713LC powders with the chemical composition provided in Table 1 were selected for the investigation. Fig. 1 depicts the homogeneous spherical shaped particles of the feedstock powder. The particle size distribution of the powder was in the range 20–63 μm.

The first section of the current work involved the processing of the Ni-based superalloys under standard PBF-LB system without any preheating conditions, to verify the cracking susceptibility of the alloys. A Renishaw AM250 system equipped with a reduced build volume device was initially adopted, using a pulsed fiber laser with a maximum power of 200 W. Based on preliminary process optimization, the hatch spacing was set to 50 μm for both alloys while a point distance of 70 and 85 μm was used for the CM247LC and IN713LC alloy, respectively. The layer thickness was fixed to 40 μm and a meander scanning strategy with a 67° rotation angle was implemented for both alloys.

Cubic-shaped specimens having a side of 10 mm length were produced and sectioned along the vertical direction (Z-axis, parallel to build direction) for the evaluation of crack density and microstructural analyses. The presence of cracks was assessed after grinding and polishing according to standard metallographic procedures. The microstructural features were highlighted after etching the polished specimens with Kalling's II reagent and examined by a Nikon Eclipse LV150NL optical microscope and by a Zeiss Sigma 500 VP field-emission scanning electron microscope (FE-SEM) equipped with energy-dispersive X-ray spectroscopy (EDS). Electron Backscatter Diffraction (EBSD) analyses were also performed after preparing selected samples with vibratory polishing technique. Information about crack development after PBF-LB was also acquired from analyses of top surfaces of the as-built samples, collecting views about the morphology of the uppermost laser tracks.

The subsequent part of this investigation concerned the effects of preheating on cracking susceptibility of the investigated alloys considering temperature levels exceeding 1300 °C, to identify the conditions required to fsuppress material damage and to highlight possible changes in cracking mechanisms with temperature. The selection of such high-temperature range was suggested by previous studies based on PBF-EB [3,18,19], which showed that preheating at 1025 °C and 1050 °C was not enough to fully suppress cracking, whereas PBF-LB experiments with 1200 °C preheating could yield defect-free samples [20]. To this aim, a simplified procedure was adopted, relying on laser-remelting of a preheated cast sample of the solid alloys. Preheating was produced by repeatedly scanning a rectangular area of 6,0 × 4,0 mm on sample surface with an Ytterbium fiber laser featuring a power of 280 W and a spot size of 191,7 μm, operated at a scanning speed of 1,35 m/s, with line offset of 0,1 mm. The hatched area was repeatedly scanned to heat up the sample to the target temperature. Once the desired temperature was reached, a further linear track was performed at 3 mm from the preheated area, producing the melting and re-solidification of the investigated alloy, as depicted in Fig. 2. Further information about the substrates and the achieved pre-heating levels are provided in Table 2. Sample temperature was monitored by using a Optris GmbH CT Laser pyrometer placed at 450 mm (the focal point of the optics) from the area of interest, pointing at the area where the single track had to be produced, with a measurement spot size of 1,5 mm. The pyrometer features a thermal sensitivity of 0,2 °C with a measuring range of 800–2200 °C and was operated with an exposure time of 1 ms. In Figs. 3a to 3(d), the recorded cooling curves measured by the pyrometer and the corresponding cooling rates are plotted.

After sample sectioning with a precision diamond-blade saw, top views and cross sections of the single tracks were analysed similarly to the PBF-LB samples for crack detection and microstructure characterization.

Finally, to support the understanding of the solidification mechanisms in the discussion of experimental results, The Thermo-Calc software (Thermo-Calc AB) was used to compute the stability of phases as a

Table 1
Chemical composition (wt.%) of the investigated CM247LC and IN713LC alloys.

Alloy	C	Cr	Co	Mo	W	Ta	Nb	Al	Ti	Hf	Zr	B	Ni
CM247LC	0,06	8,34	9,23	0,53	9,35	3,23	0,01	5,54	0,75	1,40	0009	0016	bal.
IN713LC	0,05	11,48	-	4,43	-	-	1,88	5,97	0,67	-	0125	0008	bal.

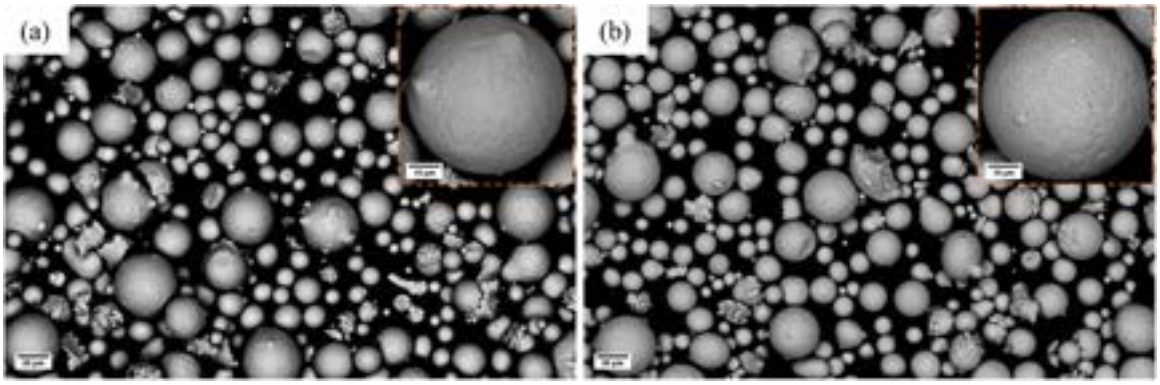

Fig. 1. SEM images of the powder morphology of (a) CM247LC and (b) IN713LC alloys.

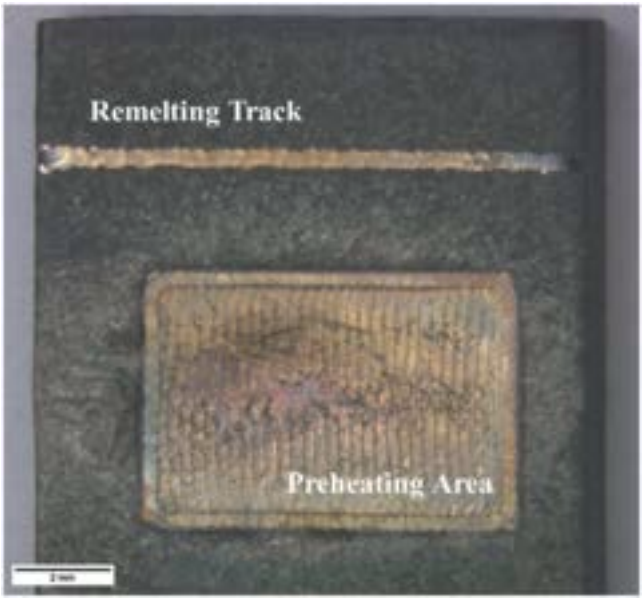

Fig. 2. View of a sample used for the high temperature remelting experiments.

Table 2
Mass of substrates for the remelting experiments and achieved preheating temperatures.

Alloy	Mass of Substrate	Preheating Level
CM247LC	3,75 g	No preheating
	4,76 g	925 °C
	2,85 g	1330 °C
	3,72 g	1339 °C
IN713LC	2,77 g	No preheating
	2,77 g	900 °C
	1,40 g	1230 °C
	2,10 g	1310 °C
	2,10 g	1330 °C

function of temperature under equilibrium and according to solidification conditions dictated by the Scheil-Gulliver model, relying on both TCNI12 and MOBNI6 databases.

3. Results

3.1. Microstructure of alloys processed by standard PBF-LB

Top surface views of the PBF-LB processed CM247LC and IN713LC specimens are depicted in Figs. 4 and 5, respectively. In the low magnification images (Figs. 4a and 5a), the parallel laser tracks can be recognized along with occasional spatters formed as a result of liquid droplets ejection from the melt pool due to interaction with the laser beam [27,28]. In the CM247LC alloy, the boundaries of the tracks are also highlighted due to the segregation of oxide slags [29] rich in Al and Hf (Fig. 4b). On the contrary, the IN713LC alloy shows more fragmented oxide films and oxide globules rich in Al and Zr, which floated on the surface of the melt pools during solidification, without being segregated at their edges (Fig. 5b).

A common feature observed on the top views of the printed samples is the abundant presence of cracks, crossing one or more tracks, oriented transversally to the scanning direction (vertical direction in the figures). Cracks were also recognized on sectioned samples, as reported in Fig. 6. For both alloys, the optical micrographs revealed a solidification structure consisting of fairly coarse columnar grains growing along the build direction (vertical in the figures). Cracks were intergranular in nature and grew crossing several melt pools with a length in the range of 100–500 μm.

The microstructure of the as-built alloys consisted of the already mentioned coarse columnar grains containing a substructure made of cells with submicrometric size, as depicted in the high-magnification FE-SEM micrographs of Fig. 7. EDS elemental maps showed that the cell boundaries were generally enriched in Hf and W for the CM247LC alloy and in Mo and Nb for the IN713LC alloy. Although no reliable quantitative evaluation could be collected at such microstructural size level by EDS, it can be qualitatively stated that the amount of segregation was higher in the CM247LC alloy whereas in the IN713LC alloy only faint increase in concentration of Mo and Nb could be detected at very high number of EDS counts.

Further data about crack development and microstructure of the CM247LC are collected in Fig. 8. It is confirmed that the cracks generally run along the grain boundaries, affecting a plurality of grains, in agreement with results already shown in Fig. 6. The EBSD analyses highlighted the presence of two types of grain morphologies after PBF-LB. Textured columnar grains are dominant in the microstructure while few near-equiaxed grains (less than 5 μm in size) could also be detected, typically close to melt pool boundaries, as also shown in the optical micrograph of Fig. 6(b) and (d). Moreover, it was found that the Hf and Ta were occasionally segregated at the grain boundaries and were consequently exposed at the faces of the opened cracks, as shown in Fig. 8(d).

3.2. Microstructure of alloys remelted by single laser tracks with high temperature preheating

The results about the processability of the investigated alloys by standard PBF-LB systems clearly showed that extensive hot cracking always took place upon rapid solidification. Literature reviews confirm that it is impossible to fully eliminate such cracks in non-weldable Ni-

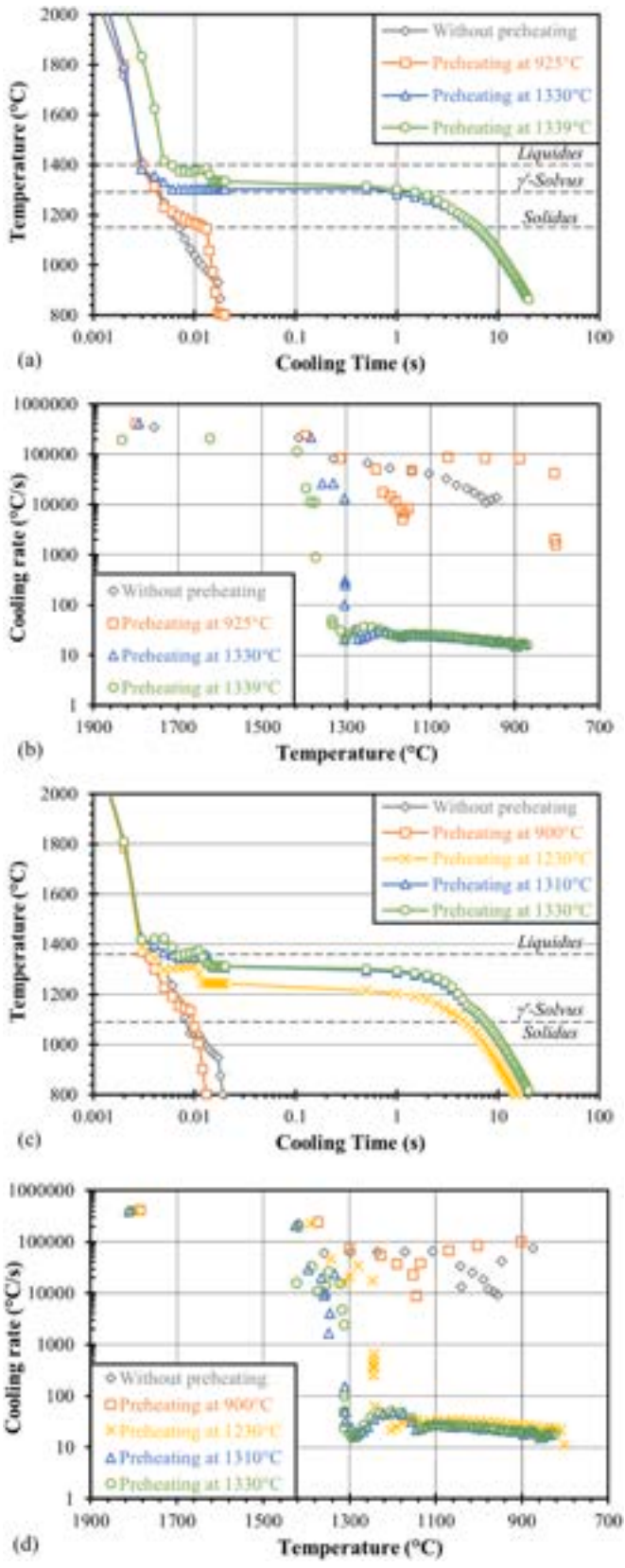

Fig. 3. Cooling curves and cooling rate trends of the remelted tracks recorded for the (a-b) CM247LC and the (c-d) IN713LC alloys.

based alloys by only optimizing the process parameters [5]. A solution for improved processability would therefore imply alloy modification, targeting the control of the critical temperature range where a small amount of liquid is found at the dendrite boundaries, and the reduction of the residual stress field by controlling the cooling rate through proper preheating.

A preliminary investigation about the preheating effects was therefore planned, extending the temperature levels well above the preheating limits of current commercial PBF-LB systems, especially considering the range of 900–1350 °C. The tests have been carried out using a simplified simulation of the PBF-LB process, starting from laser-preheated solid blocks of cast alloys (instead of a powder bed) and performing single remelting tracks instead of remelting a multilayer volume using a scanning strategy. The adoption of this approach, although leading to some discrepancies with respect to the actual PBF-LB process, allows collecting useful information about possible opportunities to mitigate hot cracking in critical alloys by a simplified setup and with reduced experimental efforts. It can also be considered that single-track remelting has been extensively used in the literature as a means for the evaluation of the Laser processability of materials. As a rule, a pre-placed powder layer is remelted by a Laser track to better simulate the process [30–32], however in the present case, extensive and homogeneous preheating would not have been possible with a powder bed due to poor conductivity of the loose powder particles with respect to bulk alloys.

In Fig. 9, stereo-micrographic images of the upper surface of single tracks generated without any preheating of the investigated alloys are depicted. Additional images about the macroscopic aspect of single tracks produced with preheating at different levels are provided in Figs. S1 and S2 of the Supplementary data. By the control tests carried out without preheating it is confirmed that extensive cracking formed in both the investigated alloys. Even after implementing preheating at 900 °C, longitudinal and transverse cracks were still observed on the track surfaces of both the investigated alloys. It is only when the preheating temperatures was raised above 1200 °C that a successful suppression of hot cracks in the CM247LC and IN713LC specimens could be achieved.

Figs. 10 and 11 contain a selection of optical micrographs showing transversal sections of the single-tracks produced at various pre-heating temperatures of the CM247LC and IN713LC alloys, respectively. The micrographs reveal the dependency of both width and depth of the melt pools on the preheating temperature, increasing with it, as expected. It is also observed that at preheating levels exceeding 900 °C, the cast structure of the substrate progressively experienced precipitate dissolution due to the solution annealing effect brought by the preheating. A statistical evaluation carried out on three different sections per condition of the unpolished samples allowed to confirm that for both the investigated alloys, preheating at 900 °C still led to frequent hot cracks, whereas temperature levels of 1200 °C and above could totally suppress the formation of such defects.

Representative FE-SEM micrographs of the single-track sections are depicted in Figs. 12 and 13. It is observed that cracks generally grew crossing a large fraction of the remelted volume, along the intergranular paths created by the grains that nucleated by an epitaxial mechanism from the unmelted substrate.

Representative elemental maps reporting the segregation patterns in the single tracks performed by 925 °C and 1339 °C preheating of the CM247LC alloy are provided in Fig. 14. It can be readily observed that by preheating at 925 °C, the cell boundaries of the melt pools are still enriched in Al and Ti, presumably stimulating the early precipitation of the γ' phase. Moreover, it was found that also Hf tends to segregate at the cell boundaries promoting the precipitation of carbides. It is noteworthy mentioning that this phenomenon was also observed in the PBF-LB microstructures reported in Figs. 7(a) and 8(d). On the contrary, the preheating level of 1339 °C was able to offer lower cooling rates (estimated to be at around 30 °C/s based on data presented in Fig. 3) within

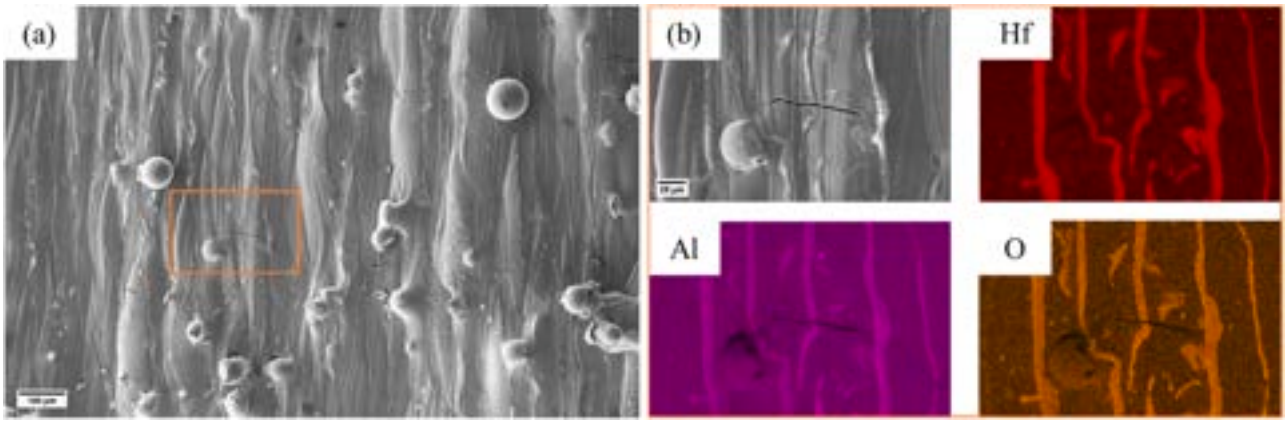

Fig. 4. Upper surface of a PBF-LB processed CM247LC alloy sample (a) low-magnification view of top surface, (b) details of a surface crack and of oxide segregation.

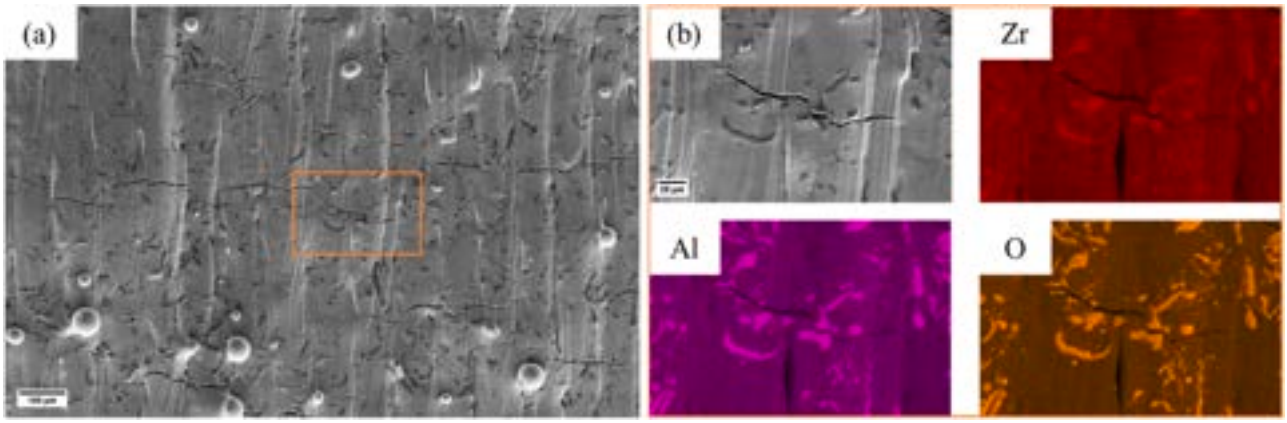

Fig. 5. Upper surface of a PBF-LB processed IN713LC alloy sample (a) low-magnification view of top surface and (b) details of a surface crack and of oxide particles.

the solidification range. This condition allowed achieving a more homogenous distribution of the γ'-former elements as well as of Hf within the microstructure, as shown in Fig. 14(b).

4. Discussion

The CM247LC and IN713LC alloys are both classified as non-weldable grades in the literature, mainly because of their tendency to promote hot cracks during last stages of solidification and due to the extensive γ' precipitation related to the large contents of Ti and Al. This phenomenon was readily confirmed by the preliminary tests conducted in the first part of the investigation using a standard PBF-LB equipment.

The expected phases formed in the investigated alloys under equilibrium as a function of temperature can be evaluated by thermodynamic calculations and are summarized in Fig. 15. It is found that the equilibrium solidification ranges are 80 °C (from 1400° to 1320°C) and 95 °C (from 1360° to 1265°C) for the CM247LC and the IN713LC alloy, respectively. Moreover, carbides and borides could also exist in the last stages of solidification. The γ' precipitation is expected under equilibrium at the solid-state, below 1270 °C and 1145 °C for the CM247LC and IN713LC alloy, respectively.

However, it is well known that Laser processing induces rapid cooling rates that lead to solidification microstructures which are far away from equilibrium condition. The Scheil-Gulliver solidification model, that assumes lack of diffusion in the solid phases and equilibrium distribution of elements at the solid-liquid interface is often adopted in the simulations of PBF-LB processes [33,34]. The calculations carried out under these conditions are summarized in Fig. 16. The data demonstrate that the solidus temperature shifts for the investigated alloys by around 170 °C below the equilibrium temperature due to elemental segregation and the corresponding increase in the amounts of low-melting phases. According to the simulation data, also summarized in Table 3, the γ/γ' eutectics is expected to precipitate during the rapid solidification in the CM247LC alloy, while Hf- and Nb-carbides and borides can potentially form, still in presence of a considerable amount of liquid, in the CM247LC and in the IN713LC alloy, respectively.

The experimental results collected by analyses on samples processed either by standard PBF-LB or by single tracks without any preheating are in full agreement with these simulations. Hf, W and Ta were found in higher concentrations at the solidification cell boundaries of the CM247LC alloy, whereas Mo and Nb slightly increased their concentration at boundaries of the IN713LC alloy.

In a second part of the investigation, emphasis was given to the effect of preheating to high temperature levels on hot-cracking susceptibility of the alloys, to verify if the reduced precipitation and limited extent of shrinkage stresses could lead to crack free samples.

The single-track Laser tests carried out at 900 and 925 °C did not significantly modified the solidification microstructure found after Laser remelting. As a result, in both alloys a significant amount of cracks was detected. It was only at very high preheating levels, close to solidus temperatures, that a change in cracking susceptibility was noticed due to the significant modification of the solidification conditions. Firstly, the high-temperature preheating allows reducing the solidification rate, as confirmed by the experimental data plotted in Fig. 3. It was measured that the laser tracks performed without preheating and with preheating at 900 and 925 °C featured cooling rates in the range of 10^4-10^6 °C/s within the solidification interval, which is in good agreement with expected data provided in the literature for standard PBF-LB processes [1].

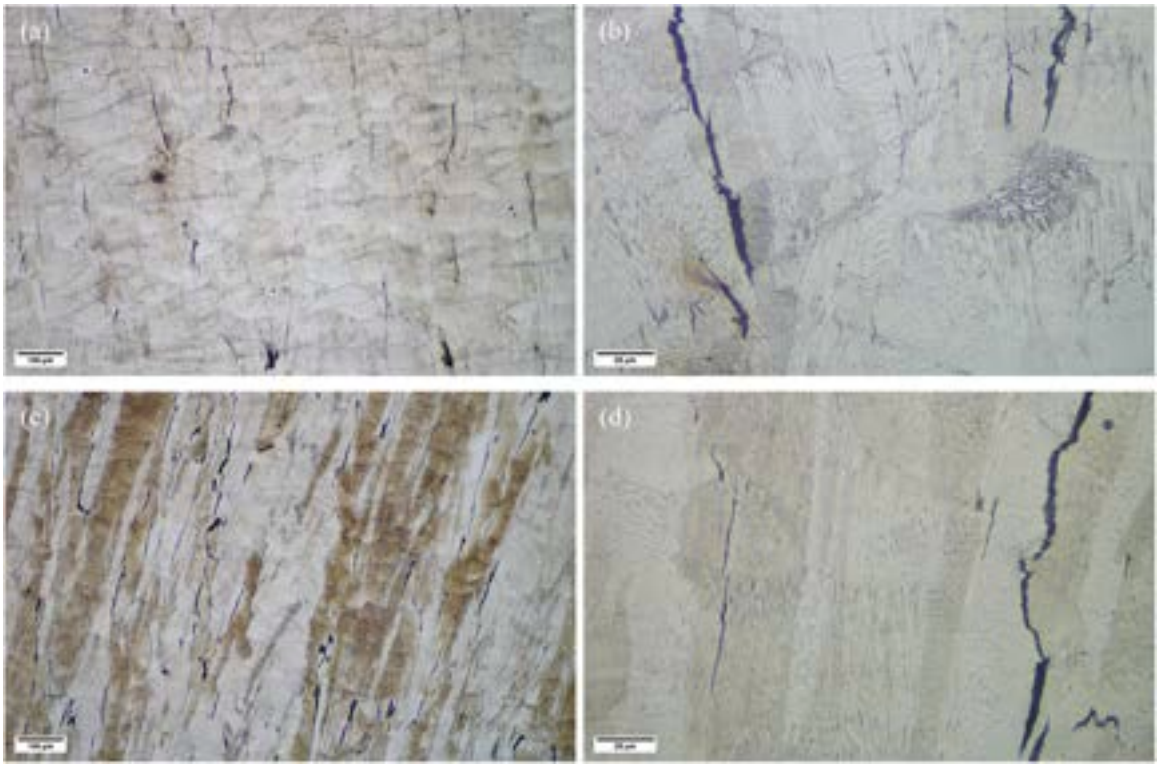

Fig. 6. Optical micrographs of vertically sectioned samples of the PBF-LB processed (a-b) CM247LC and (c-d) IN713LC alloys.

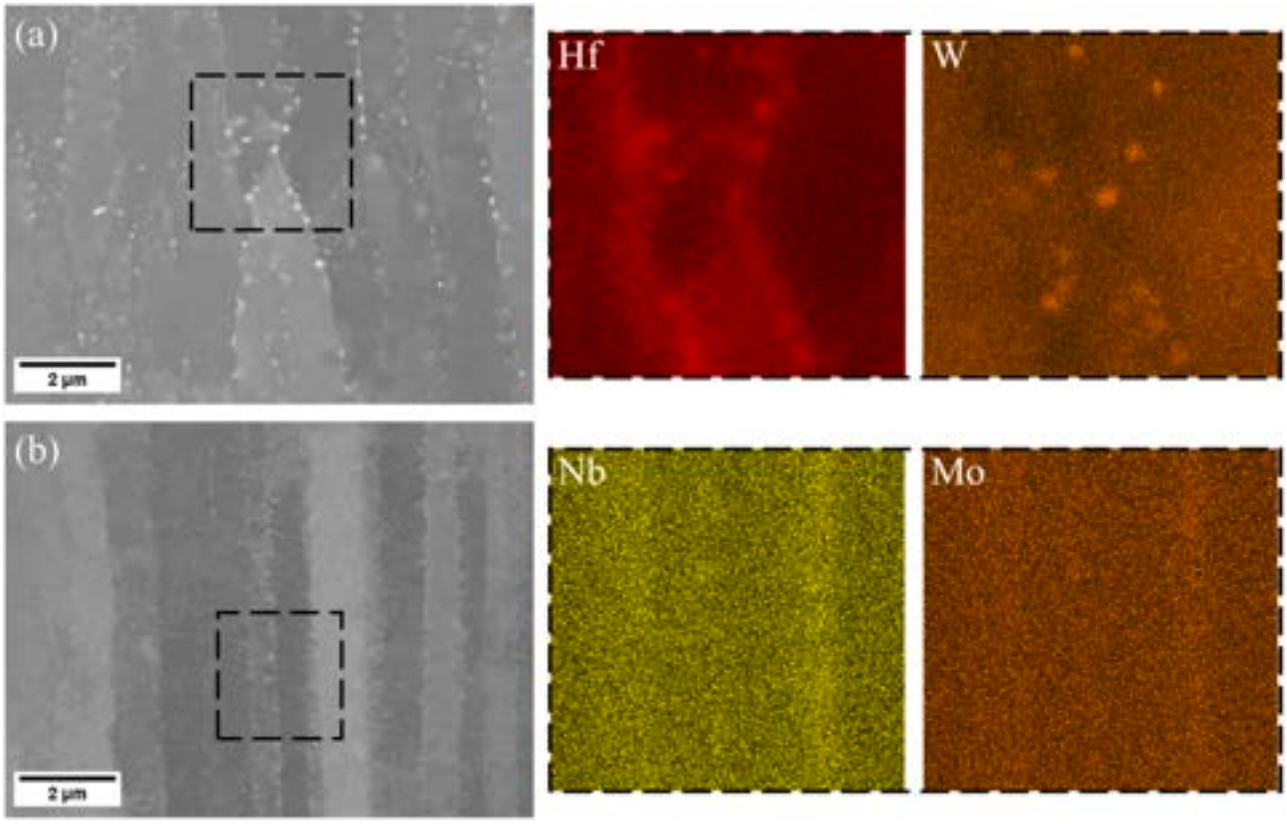

Fig. 7. Details of the fine cellular structure with micro-segregation and precipitation of secondary phases in the (a) CM247LC alloy with Hf and W maps, and (b) IN713LC alloy with Nb and Mo maps (vertically sectioned samples),.

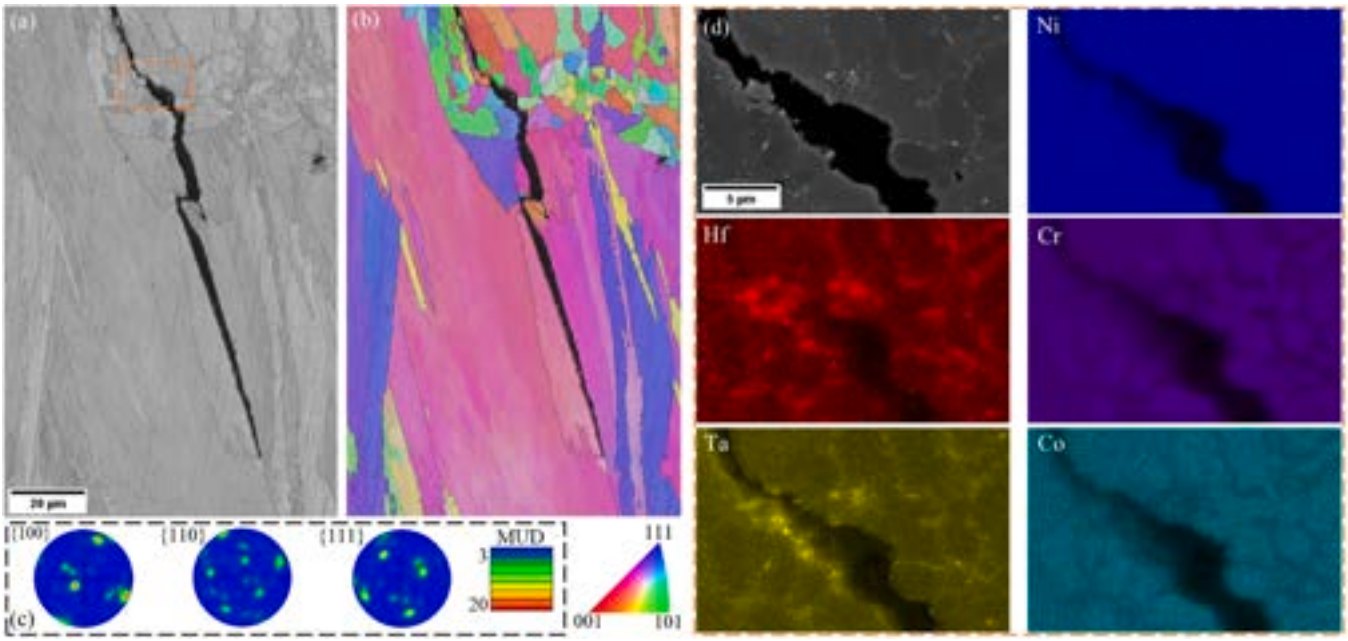

Fig. 8. EBSD images collected close to a crack in the CM247LC alloy: (a) band contrast, (b) and (c) orientation map and calculated pole figures, (d) elemental map analysis around the crack zone highlighted in the band contrast image.

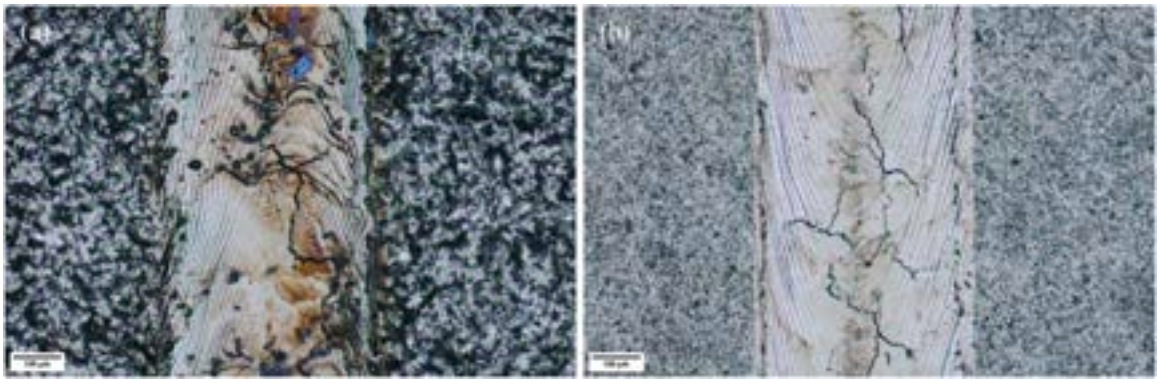

Fig. 9. Views of the remelting laser tracks carried out on samples without preheating. (a) CM247LC and (b) IN713LC alloys.

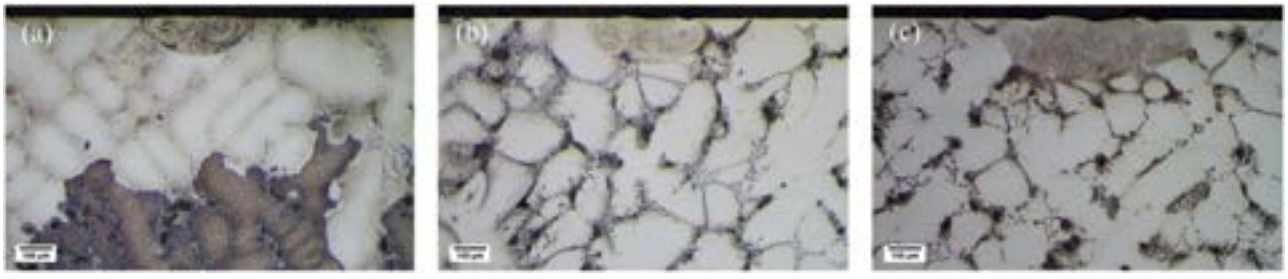

Fig. 10. Single-track melt pool sections of the CM247LC alloy with preheating of (a) 925 °C, (b) 1300 °C and (c) 1339 °C.

On the contrary, preheating above 1200 °C allowed slowing down to a significant extent the cooling rate within the solidification interval, hence reducing segregation. A second effect brought about by the extensive preheating consists in the ability to hold the temperature slightly above the solidus temperature and the γ'-solvus level for a longer period, of the order of a few seconds for the specific experimental setup here considered (see Fig. 3a and c). These combined effects are assumed to be beneficial in view of the ability to relax shrinkage stresses and improve the backfilling ability of the liquid in the cavities formed in the mushy zone in the last stages of solidification. In addition, the grain-boundary segregation of carbide/boride former elements would be mitigated at the stage where they might become particularly critical for the hot-cracking phenomena.

Therefore, one of the main outcomes of this investigation is the evidence that preheating levels above about 1200 °C, even exceeding the alloy solidus and γ'-solvus temperatures, are required to fully suppress hot cracking phenomena in the most critical Ni-based alloys. Considering possible options for implementing such high-temperature

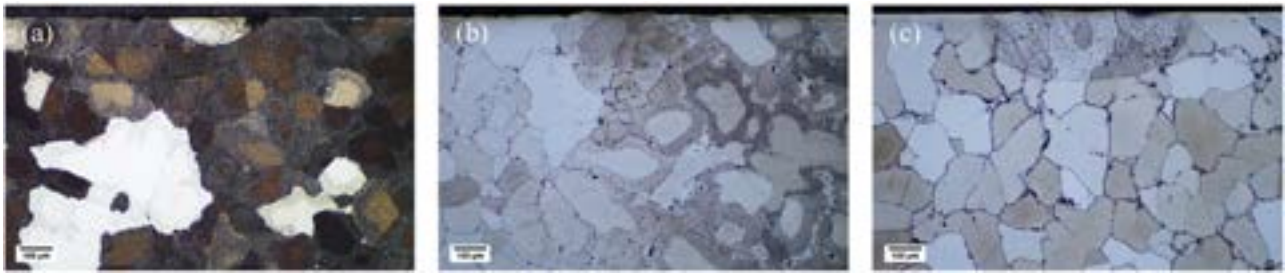

Fig. 11. Single-track melt pool sections of the IN713LC alloy with preheating of (a) 900 °C, (b) 1230 °C and (c) 1330 °C.

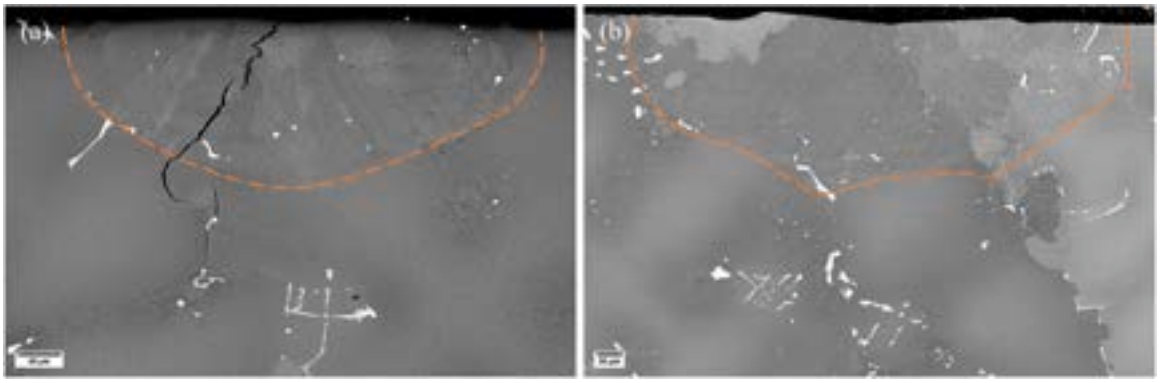

Fig. 12. Single-track melt pool sections obtained by preheating the CM247LC alloy at 925 °C (a) and at 1339 °C (b). The melt pool shapes are highlighted by the orange lines.

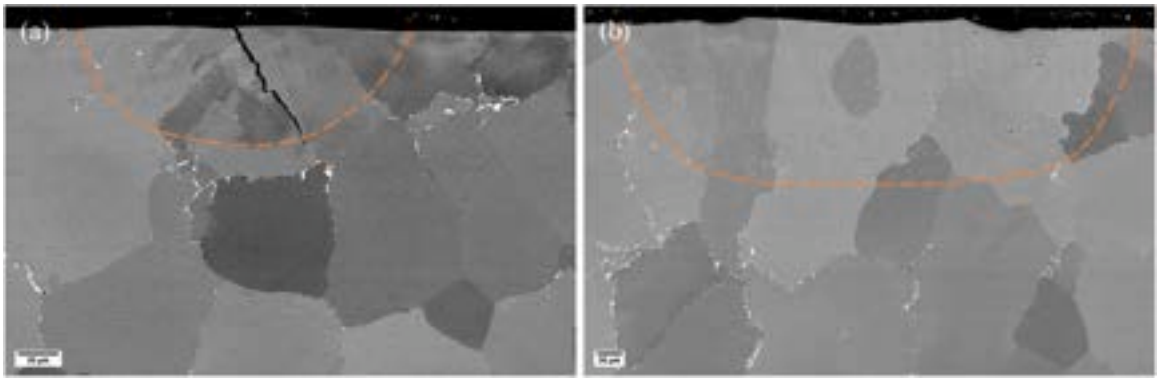

Fig. 13. Single-track melt pool sections obtained by preheating the IN713LC alloy at 900 °C (a) and at 1330 °C (b). The melt pool shapes are highlighted by the orange lines.

preheating conditions in a conventional PBF-LB equipment to be used for the manufacturing of real parts, it can be argued that such an extensive heating of the full powder bed volume is obviously impracticable. On the contrary, a more feasible option could be the development of a proper Laser-beam shaping or beam splitting approach to promote suitable local pre-heating and/or post-heating effects to the powder bead and to the consolidated alloy, respectively, in order to mitigate the critical solidification conditions. Finally, it can be speculated that these approaches could more conveniently be developed jointly to alloy chemistry optimization and further tuning of process parameters to improve the overall printability of the investigated high-strength Ni-based superalloys.

5. Conclusions

The current study was aimed at investigating the hot-cracking mechanisms during PBF-LB processing of the γ'-strengthened CM247LC and IN713LC alloys and to evaluate the effectiveness of mitigation criteria for the reduction of hot cracking phenomena. The main conclusions of this work could be drawn as follows.

- A single-track Laser remelting approach was developed to investigate the effects of high-temperature preheating. Remelting without preheating led to the expected hot cracking in both alloys, producing hot tears with features comparable to those found by conventional PBF-LB processing.
- Cracks were still observed even after applying preheating levels up to 925 °C. The experimental measurements of the thermal history during processing showed that the cooling rates were above 10^4 °C/s, resulting in the segregation of alloying elements and extensive enrichments of γ'- and carbide/boride-former elements at the boundaries of the solidified cells.
- It was demonstrated that preheating levels above about 1200 °C are required to fully suppress hot cracking phenomena in the

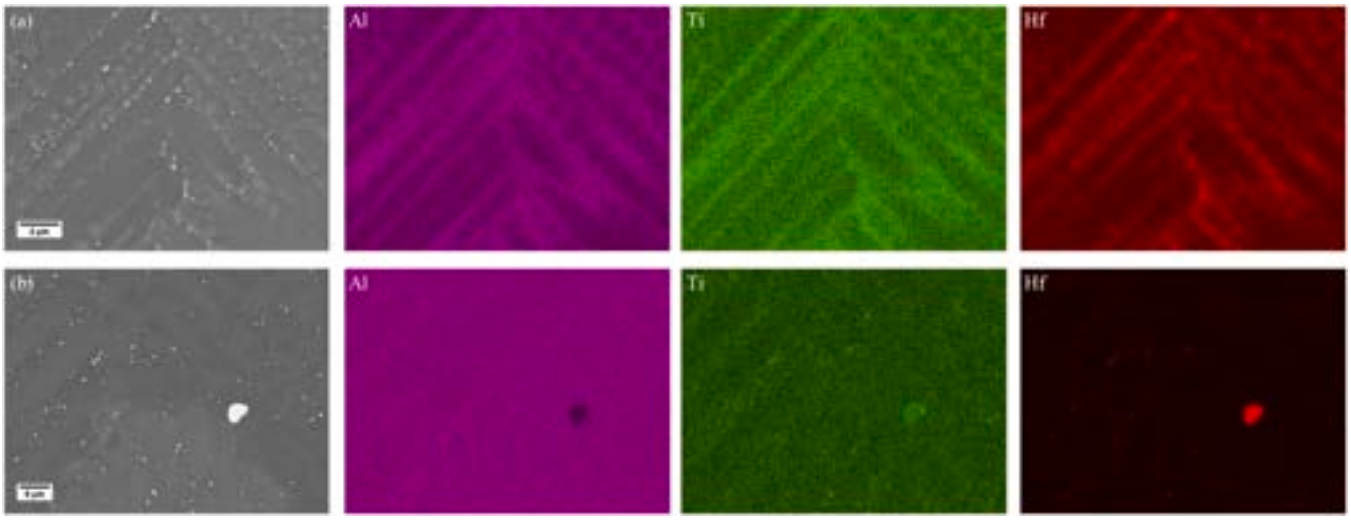

Fig. 14. Elemental maps for the CM247LC alloy single tracks at a preheating condition of (a) 925 °C and (b) 1339 °C.

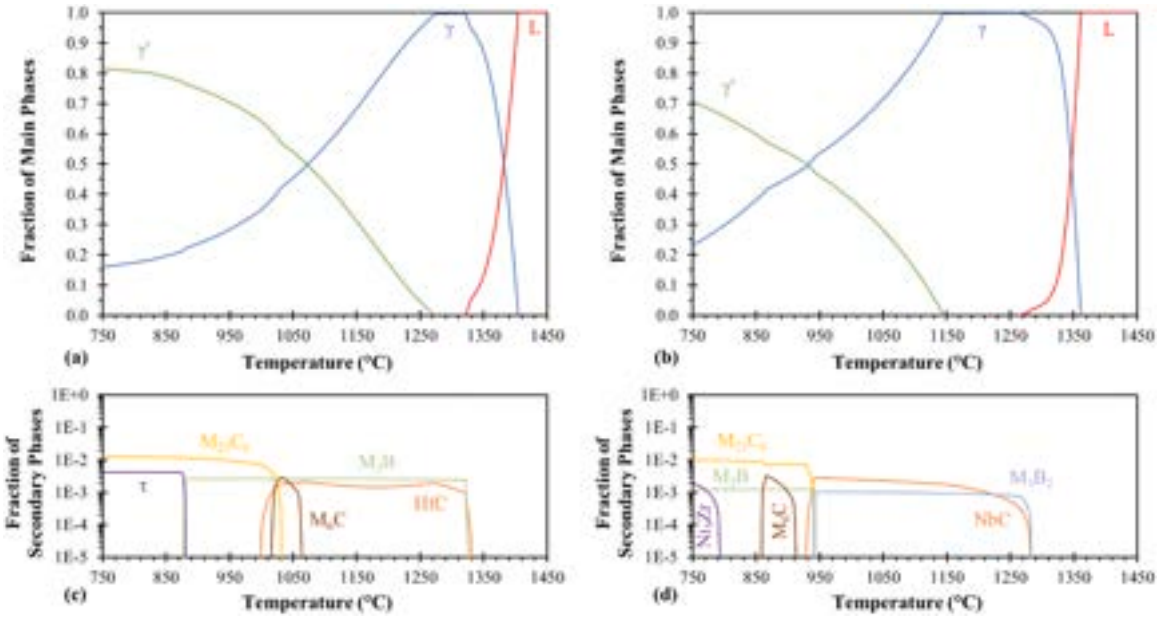

Fig. 15. Equilibrium stability of the main phases for the (a) CM247LC alloy and (b) IN713LC alloy. (c) and (d) represent the amount of equilibrium secondary phases in CM247LC and IN713LC alloys respectively.

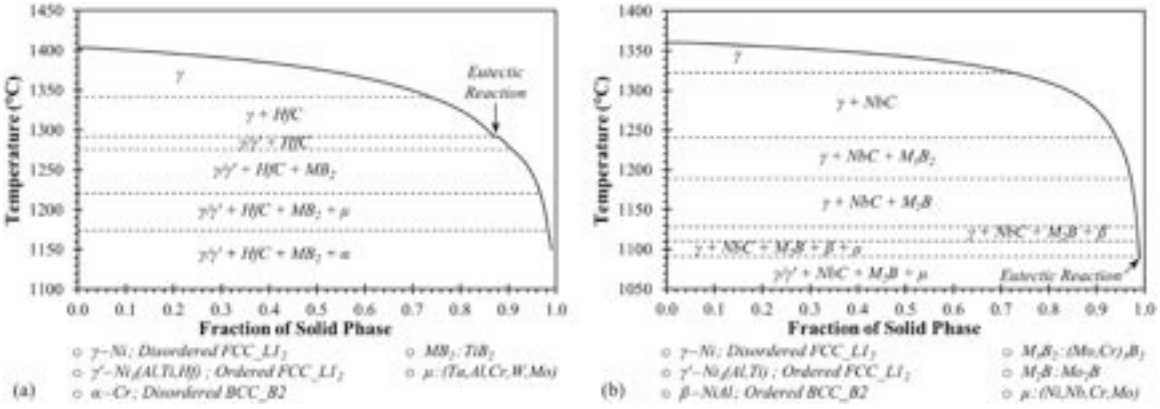

Fig. 16. Solidification sequence according to Scheil-Gulliver solidification model for the (a) CM247LC and (b) IN713LC alloys.

Table 3
Main transformation temperatures of the investigated CM247LC and IN713LC alloys obtained from the thermodynamic simulations.

Alloy	Condition	Liquidus Temperature	Solidus Temperature	Solidification range	γ' precipitates		MC precipitates	
					Formation Temperature	Solid Fraction	Formation Temperature	Solid Fraction
CM274LC	Equilibrium	1400 °C	1320 °C	80 °C	1270 °C	Solid-State	1330 °C	94 %
	Scheil-Gulliver model	1400 °C	1150 °C	250 °C	1290 °C	87%	1340 °C	74 %
IN713LC	Equilibrium	1360 °C	1265 °C	95 °C	1145 °C	Solid-State	1280 °C	98 %
	Scheil-Gulliver model	1360 °C	1090 °C	270 °C	1090 °C	99%	1322 °C	73 %

investigated alloys. The reduced solidification rate and the relatively longer period spent above the solidus and γ'-solvus temperatures were assumed to be beneficial in view of the improved filling ability of the liquid in the cavities formed in the mushy zone in the last stages of solidification and the ability to relax shrinkage stresses.

Finally, it is noteworthy to mention that a high-temperature pre-heating of the powder bed to 1200 °C can hardly be implemented into a standard PBF-LB system. A more feasible option could be the development of laser-beam shaping or laser-beam splitting approaches to promote suitable local pre-heating and/or post-heating to the alloy, to mitigate the critical solidification conditions.

Author statement

All authors have approved the manuscript and agree with its submission to Materials Today Communications.

Declaration of Competing Interest

The authors declare that they have no known competing financial interests or personal relationships that could have appeared to influence the work reported in this paper.

Data Availability

Data will be made available on request.

Acknowledgements

The investigation was performed in the frame of joint research project CUSTODIAN - Customized photonic devices for defectless laser based manufacturing (Grant agreement ID: 825103), funded by H2020-ICT in 2018–2022.

Appendix A. Supporting information

Supplementary data associated with this article can be found in the online version at doi:10.1016/j.mtcomm.2023.107644.

References

[1] T. DebRoy, H.L. Wei, J.S. Zuback, T. Mukherjee, J.W. Elmer, J.O. Milewski, A. M. Beese, A. Wilson-Heid, A. De, W. Zhang, Additive manufacturing of metallic components – process, structure and properties, Prog. Mater. Sci. 92 (2018) 112–224, https://doi.org/10.1016/J.PMATSCI.2017.10.001.

[2] R.C. Reed, C.M.F. Rae, Physical metallurgy of the nickel-based superalloys, Phys. Metall. Fifth Ed. 1 (2014) 2215–2290, https://doi.org/10.1016/B978-0-444-53770-6.00022-8.

[3] E. Chauvet, P. Kontis, E.A. Jägle, B. Gault, D. Raabe, C. Tassin, J.J. Blandin, R. Dendievel, B. Vayre, S. Abed, G. Martin, Hot cracking mechanism affecting a non-weldable Ni-based superalloy produced by selective electron Beam Melting, Acta Mater. 142 (2018) 82–94, https://doi.org/10.1016/J.ACTAMAT.2017.09.047.

[4] L.N. Carter, M.M. Attallah, R.C. Reed, Laser powder bed fabrication of nickel-base superalloys: Influence of parameters; characterisation, quantification and mitigation of cracking, Proc. Int. Symp. Superalloys (2012), https://doi.org/10.7449/2012/superalloys_2012_577_586.

[5] O. Adegoke, J. Andersson, H. Brodin, R. Pederson, Review of laser powder bed fusion of gamma-prime-strengthened nickel-based superalloys, Metals (Basel) 10 (2020), https://doi.org/10.3390/met10080996.

[6] S. Griffiths, H. Ghasemi Tabasi, T. Ivas, X. Maeder, A. De Luca, K. Zweiacker, R. Wróbel, J. Jhabvala, R.E. Logé, C. Leinenbach, Combining alloy and process modification for micro-crack mitigation in an additively manufactured Ni-base superalloy, Addit. Manuf. 36 (2020), 101443, https://doi.org/10.1016/J.ADDMA.2020.101443.

[7] H. Wang, X. Zhang, G.B. Wang, J. Shen, G.Q. Zhang, Y.P. Li, M. Yan, Selective laser melting of the hard-to-weld IN738LC superalloy: efforts to mitigate defects and the resultant microstructural and mechanical properties, J. Alloy. Compd. 807 (2019), 151662, https://doi.org/10.1016/J.JALLCOM.2019.151662.

[8] M. Zhong, H. Sun, W. Liu, X. Zhu, J. He, Boundary liquation and interface cracking characterization in laser deposition of Inconel 738 on directionally solidified Ni-based superalloy, Scr. Mater. 53 (2005) 159–164, https://doi.org/10.1016/J.SCRIPTAMAT.2005.03.047.

[9] C. Qiu, H. Chen, Q. Liu, S. Yue, H. Wang, On the solidification behaviour and cracking origin of a nickel-based superalloy during selective laser melting, Mater. Charact. 148 (2019) 330–344, https://doi.org/10.1016/J.MATCHAR.2018.12.032.

[10] M. Mohsin Raza, Y.L. Lo, Experimental investigation into microstructure, mechanical properties, and cracking mechanism of IN713LC processed by laser powder bed fusion, Mater. Sci. Eng. A 819 (2021), 141527, https://doi.org/10.1016/J.MSEA.2021.141527.

[11] A. Chamanfar, M. Jahazi, A. Bonakdar, E. Morin, A. Firoozrai, Cracking in fusion zone and heat affected zone of electron beam welded Inconel-713LC gas turbine blades, Mater. Sci. Eng. A 642 (2015) 230–240, https://doi.org/10.1016/J.MSEA.2015.06.087.

[12] X. Wang, L.N. Carter, B. Pang, M.M. Attallah, M.H. Loretto, Microstructure and yield strength of SLM-fabricated CM247LC Ni-Superalloy, Acta Mater. 128 (2017) 87–95, https://doi.org/10.1016/J.ACTAMAT.2017.02.007.

[13] O. Adegoke, J. Andersson, H. Brodin, R. Pederson, Influence of laser powder bed fusion process parameters on voids, cracks, and microhardness of nickel-based superalloy alloy 247LC, Materials (Basel) 13 (2020), https://doi.org/10.3390/MA13173770.

[14] J.H. Boswell, D. Clark, W. Li, M.M. Attallah, Cracking during thermal post-processing of laser powder bed fabricated CM247LC Ni-superalloy, Mater. Des. 174 (2019), 107793, https://doi.org/10.1016/J.MATDES.2019.107793.

[15] R. Muñoz-Moreno, V.D. Divya, S.L. Driver, O.M.D.M. Messé, T. Illston, S. Baker, M. A. Carpenter, H.J. Stone, Effect of heat treatment on the microstructure, texture and elastic anisotropy of the nickel-based superalloy CM247LC processed by selective laser melting, Mater. Sci. Eng. A 674 (2016) 529–539, https://doi.org/10.1016/J.MSEA.2016.06.075.

[16] V.D. Divya, R. Muñoz-Moreno, O.M.D.M. Messé, J.S. Barnard, S. Baker, T. Illston, H.J. Stone, Microstructure of selective laser melted CM247LC nickel-based superalloy and its evolution through heat treatment, Mater. Charact. 114 (2016) 62–74, https://doi.org/10.1016/J.MATCHAR.2016.02.004.

[17] J.N. Ghoussoub, Y.T. Tang, W.J.B. Dick-Cleland, A.A.N. Németh, Y. Gong, D. G. McCartney, A.C.F. Cocks, R.C. Reed, On the influence of alloy composition on the additive manufacturability of Ni-based superalloys, Metall. Mater. Trans. A Phys. Metall. Mater. Sci. 53 (2022), https://doi.org/10.1007/s11661-021-06568-z.

[18] H. Peng, Y. Shi, S. Gong, H. Guo, B. Chen, Microstructure, mechanical properties and cracking behaviour in a γ'-precipitation strengthened nickel-base superalloy fabricated by electron beam melting, Mater. Des. 159 (2018) 155–169, https://doi.org/10.1016/J.MATDES.2018.08.054.

[19] Y.S. Lee, M.M. Kirka, S. Kim, N. Sridharan, A. Okello, R.R. Dehoff, S.S. Babu, AsymmeTric Cracking in Mar-M247 alloy builds during electron beam powder bed fusion additive manufacturing, Metall. Mater. Trans. A Phys. Metall. Mater. Sci. 49 (2018), https://doi.org/10.1007/s11661-018-4788-8.

[20] Y.C. Hagedorn, J. Risse, W. Meiners, N. Pirch, K. Wissenbach, R. Poprawe, Processing of nickel based superalloy MAR M-247 by means of high temperature - selective laser melting (HT - SLM), High. Value Manuf. Adv. Res. Virtual Rapid Prototyp. - Proc. 6th Int. Conf. Adv. Res. Rapid Prototyp. VR@P 2014 (2013), https://doi.org/10.1201/b15961-54.

[21] S. Griffiths, H. Ghasemi-Tabasi, A. De Luca, J. Pado, S.S. Joglekar, J. Jhabvala, R. E. Logé, C. Leinenbach, Influence of Hf on the heat treatment response of additively manufactured Ni-base superalloy CM247LC, Mater. Charact. 171 (2021), 110815, https://doi.org/10.1016/J.MATCHAR.2020.110815.

[22] C. Guo, G. Li, S. Li, X. Hu, H. Lu, X. Li, Z. Xu, Y. Chen, Q. Li, J. Lu, Q. Zhu, Additive manufacturing of Ni-based superalloys: residual stress, mechanisms of crack formation and strategies for crack inhibition, Nano Mater. Sci. 5 (2023) 53–77, https://doi.org/10.1016/J.NANOMS.2022.08.001.
[23] Q. Han, Y. Gu, R. Setchi, F. Lacan, R. Johnston, S.L. Evans, S. Yang, Additive manufacturing of high-strength crack-free Ni-based Hastelloy X superalloy, Addit. Manuf. 30 (2019), 100919, https://doi.org/10.1016/J.ADDMA.2019.100919.
[24] N.J. Harrison, I. Todd, K. Mumtaz, Reduction of micro-cracking in nickel superalloys processed by selective laser melting: a fundamental alloy design approach, Acta Mater. 94 (2015) 59–68, https://doi.org/10.1016/J.ACTAMAT.2015.04.035.
[25] Y. Zhao, Z. Ma, L. Yu, Y. Liu, New alloy design approach to inhibiting hot cracking in laser additive manufactured nickel-based superalloys, Acta Mater. 247 (2023), 118736, https://doi.org/10.1016/J.ACTAMAT.2023.118736.
[26] N. Kalentics, N. Sohrabi, H.G. Tabasi, S. Griffiths, J. Jhabvala, C. Leinenbach, A. Burn, R.E. Logé, Healing cracks in selective laser melting by 3D laser shock peening, Addit. Manuf. 30 (2019), 100881, https://doi.org/10.1016/J.ADDMA.2019.100881.
[27] A.N.D. Gasper, B. Szost, X. Wang, D. Johns, S. Sharma, A.T. Clare, I.A. Ashcroft, Spatter and oxide formation in laser powder bed fusion of Inconel 718, Addit. Manuf. 24 (2018) 446–456, https://doi.org/10.1016/J.ADDMA.2018.09.032.
[28] M.H. Nasab, D. Gastaldi, N.F. Lecis, M. Vedani, On morphological surface features of the parts printed by selective laser melting (SLM), Addit. Manuf. 24 (2018) 373–377, https://doi.org/10.1016/J.ADDMA.2018.10.011.
[29] A. De Luca, C. Kenel, S. Griffiths, S.S. Joglekar, C. Leinenbach, D.C. Dunand, Microstructure and defects in a Ni-Cr-Al-Ti γ/γ' model superalloy processed by laser powder bed fusion, Mater. Des. 201 (2021), 109531, https://doi.org/10.1016/J.MATDES.2021.109531.
[30] A. Basak, S. Das, Microstructure of nickel-base superalloy MAR-M247 additively manufactured through scanning laser epitaxy (SLE), J. Alloy. Compd. 705 (2017) 806–816, https://doi.org/10.1016/J.JALLCOM.2017.02.013.
[31] A. Basak, S. Das, Additive manufacturing of nickel-base superalloy IN100 through scanning laser epitaxy, JOM 70 (2018), https://doi.org/10.1007/s11837-017-2638-6.
[32] R. Acharya, R. Bansal, J.J. Gambone, M.A. Kaplan, G.E. Fuchs, N.G. Rudawski, S. Das, Additive manufacturing and characterization of rené 80 superalloy processed through scanning laser epitaxy for turbine engine hot-section component repair, Adv. Eng. Mater. 17 (2015), https://doi.org/10.1002/adem.201400589.
[33] N. Sargent, M. Jones, R. Otis, A.A. Shapiro, J.P. Delplanque, W. Xiong, Integration of processing and microstructure models for non-equilibrium solidification in additive manufacturing, Metals (Basel) 11 (2021), https://doi.org/10.3390/met11040570.
[34] B. Bocklund, L.D. Bobbio, R.A. Otis, A.M. Beese, Z.K. Liu, Experimental validation of Scheil–Gulliver simulations for gradient path planning in additively manufactured functionally graded materials, Materialia 11 (2020), 100689, https://doi.org/10.1016/J.MTLA.2020.100689.